Article

Halloysite Nanotubes with Immobilized Plasmonic Nanoparticles for Biophotonic Applications

Anastasiia V. Kornilova [1], Sergey M. Novikov [2], Galiya A. Kuralbayeva [3], Subhra Jana [4], Ivan V. Lysenko [5], Anastasia I. Shpichka [6], Anna V. Stavitskaya [7], Maxim V. Gorbachevskii [7], Andrei A. Novikov [7], Saltanat B. Ikramova [8], Peter S. Timashev [6,9,10,11], Aleksey V. Arsenin [2], Valentyn S. Volkov [2], Alexander N. Vasiliev [12] and Victor Yu. Timoshenko [1,13,14,*]

1   Physics Department, Lomonosov Moscow State University, 119991 Moscow, Russia; shargenga@mail.ru
2   Center for Photonics and 2D Materials, Moscow Institute of Physics and Technology (MIPT), 141700 Dolgoprudny, Russia; novikov.s@mipt.ru (S.M.N.); arsenin.av@mipt.ru (A.V.A.); vsv.mipt@gmail.com (V.S.V.)
3   National University of Science and Technology "MISIS", 119049 Moscow, Russia; galiy.91@mail.ru
4   S. N. Bose National Centre for Basic Sciences, Kolkata 700106, India; subhra.jana@bose.res.in
5   Physics Department, Taras Shevchenko National University of Kyiv, 01601 Kyiv, Ukraine; ivan.lysenko305@gmail.com
6   World-Class Research Center "Digital Biodesign and Personalized Healthcare", Sechenov University, 119991 Moscow, Russia; shpichka_a_i@staff.sechenov.ru (A.I.S.); timashev_ps@staff.sechenov.ru (P.S.T.)
7   Functional Aluminosilicate Nanomaterials Lab, Department of Physical and Colloid Chemistry, Gubkin University, 119991 Moscow, Russia; stavitsko@mail.ru (A.V.S.); slemwen@ya.ru (M.V.G.); novikov.a@gubkin.ru (A.A.N.)
8   Faculty of Physics and Technology, Al-Farabi Kazakh National University, 71, Al-Farabi Ave., Almaty 050040, Kazakhstan; Ykramova.Saltanat@kaznu.kz
9   Institute for Regenerative Medicine, Sechenov University, 119991 Moscow, Russia
10 Department of Polymers and Composites, N.N. Semenov Federal Research Center for Chemical Physics, Russian Academy of Sciences, 119991 Moscow, Russia
11 Chemistry Department, Lomonosov Moscow State University, 119991 Moscow, Russia
12 National Research South Ural State University, 454080 Chelyabinsk, Russia; anvas2000@yahoo.com
13 Phys-Bio Institute, National Research Nuclear University "MEPhI", 115409 Moscow, Russia
14 Lebedev Physical Institute of the Russian Academy of Sciences, 119333 Moscow, Russia
*   Correspondence: timoshen@physics.msu.ru

Featured Application: Molecular sensorics and biophotonics.

Abstract: Halloysite nanotubes (HNTs) with immobilized gold (Au) and silver (Ag) nanoparticles (NPs) belong to a class of nanocomposite materials whose physical properties and applications depend on the geometry of arrangements of the plasmonic nanoparticles on HNT' surfaces. We explore HNTs:(Au, Ag)-NPs as potential nano-templates for surface-enhanced Raman scattering (SERS). The structure and plasmonic properties of nanocomposites based on HNTs and Au- and Ag-NPs are studied by means of the transmission electron microscopy and optical spectroscopy. The optical extinction spectra of aqueous suspensions of HNTs:(Au, Ag)-NPs and spatial distributions of the electric fields are simulated, and the simulation results demonstrate the corresponding localized plasmonic resonances and numerous "hot spots" of the electric field nearby those NPs. In vitro experiments reveal an enhancement of the protein SERS in fibroblast cells with added HNTs:Ag-NPs. The observed optical properties and SERS activity of the nanocomposites based on HNTs and plasmonic NPs are promising for their applications in biosensorics and biophotonics.

Keywords: halloysite; nanoparticles; plasmonics; optical properties simulation; surface-enhanced Raman scattering; biosensorics; biophotonics

1. Introduction

Halloysite is an aluminosilicate material, which is naturally structured into eco-friendly, non-toxic nanosized rolls [1,2]. The inner and outer surfaces of halloysite nanotubes (HNTs) have different surface charges [3] due to which HNTs have a wide range of applications as nanocontainers for both drug delivery [4] and other useful agents [5], and as matrices for the deposition of nanoparticles (NPs) [6]. HNT-based drug formulations demonstrate lower drug side effects, render the protection of drug molecules from possible degradation in aggressive conditions (low/high pH, enzymatic activity), increase the aqueous solubility of hydrophobic insoluble drugs, accumulate in pathological sites in the body, and help controlling drug release rates [7–9]. For example, a prodigiosin-HNT-based nanoformulation (p-HNTs) and its effects on the viability of malignant and non-malignant cells have been demonstrated [10]. NPs of plasmonic metals attached at the HNT's surface can form hot spots between each other, where local electric fields from each pair of NPs are enhanced [11,12]. Moreover, plasmonic NPs, which are fixed on HNTs, are protected from sticking together, they form agglomerates less often, and retain their properties longer [11]. Note that the physical properties of nanostructures depend on their topology-driven interface conditions, and an example of the terahertz light absorption in semiconductor nanoshells resonantly enhanced due to the strong coupling between interface plasmons and phonons is demonstrated [13].

Silver nanoparticles (Ag-NPs) are widely used as a nanomaterial with superior plasmonic properties, and the SERS activity of Ag-NPs is shown and developed in a variety of studies [14–19]. The SERS phenomenon can also allow using such NPs in the solar energy conversion systems [20] and as biosensors for the detection of different substances both in water and in vitro [17,21]. Ag-NPs deposited on the HNTs surface can result in localized surface plasmon resonance (LSPR) in the region of 400 to 600 nm [11,22] and thus it could be used for SERS [3]. It was shown that a noticeable SERS response is observed upon the addition of Rhodamine 6G dye to the HNTs:Ag-NPs nanocomposite [11]. Note, the SERS activity of HNTs:Ag-NPs persists even after soaking in aqueous solution for a week [11]. While Ag-NPs have a wide range of applications in disinfection [14], the possibility of their deposition on the HNT's matrix makes it possible to enhance the effect by combining the bactericidal action of silver ions with electric field amplification from LSPR modes [22].

Gold nanoparticles (Au-NPs) are similarly well-known for their SERS ability [23,24]. Nanocomposites based on HNTs and Au-NPs are often explored for catalytic applications [25], including precisely due to the plasmonic properties of Au-NPs [26]. Herewith, the protocol for "growing" Au-NPs on the surface of the HNTs is well-developed, since the efficiency of HNTs as SERS substrate has been proven [27]. While the SERS of Rhodamine 6G (R6G) at the concentration of 10^{-3} M was found for HNTs:Au-NPs, the reported rather low sensitivity and required large sizes on Au-NPs of about 50 nm can be limiting factors for further applications [27].

We report on the SERS activity of HNTs decorated with surface-immobilized Ag- and Au-NPs with men sizes from 5 to 10 nm. The plasmonic properties of HNTs:Au/Ag-NPs nanocomposites are also simulated to reveal the role of the NPs' geometric characteristics: size distribution and spatial localization on the nanotube' surface. The potential of the prepared nanocomposites for the SERS analysis of biosystems is demonstrated by experiments in vitro.

2. Materials and Methods

All chemicals were used as received. HNTs, silver nitrate (AgNO3, 99.9999%), tetrachloroauric acid (HAuCl$_4$·3H$_2$O, 99.9%), sodium citrate dihydrate (99%), (3-Aminopropyl) triethoxysilane (APTES, 99%), and sodium borohydride (NaBH$_4$) were purchased from Sigma-Aldrich. (3-aminopropyl) triethoxysilane (97%) Toluene was obtained from Merck. Prior immobilization of Ag- and Au-NPs the surface of HNTs was APTES-modified through grafting reaction [28]. The reaction was performed under a nitrogen atmosphere using a standard air-free technique (for details, see [22]). In order to prepare an aqueous suspension

of HNTs:Au-NPs, APTES-modified HNTs [24] were added dropwise to colloidal solution of Au-NPs, which were synthesized according to [29]. The obtained suspension was agitated and left to mix on a shaker for 12 h. Next, the samples were centrifuged, washed with de-ionized water twice, and concentrated to 1 mg/mL. The HNTs decorated with Ag-NPs were washed several times with deionized water to remove the excess borohydride and finally dried in air to obtain powder of HNTs:Ag-NPs. Then, the powder with a concentration of about 1 mg/mL was dispersed in deionized water to prepare aqueous suspensions of HNTs:Ag-NPs.

HNTs before and after immobilization of Au- and Au-NPs were investigated using a transmission electron microscope (TEM: FEI TECNAI G2 F20-ST) operating at 200 kV, after drop-casting a drop of solution of the sample onto a carbon coated copper grid. The size distributions of plasmonic NPs were obtained from their TEM images by using a free ImageJ software.

In vitro tests were carried out by using the Raman spectroscopy of cells (3T3 fibroblasts) cultivated with HNTs:Ag-NPs. The measurements were carried out by using a confocal scanning Raman microscope Horiba LabRAM HR Evolution (HORIBA Ltd., Kyoto, Japan). All measurements were performed with linearly polarized exciting light at a wavelength of 632.8 nm, 600 lines/mm diffraction grating, and $\times 100$ objective (N.A. = 0.90), whereas we used unpolarized detection to have a significant signal-to-noise ratio. The spot size was about 0.43 μm. The Raman spectra were recorded with 7.5 mW incident powers and an integration time of 30 s at each point. The statistics were collected from (at least) 25 points at different parts of the sample. SERS measurements were carried out for four sets of the samples, i.e., (i) a control set with fibroblast cells without with HNTs:Ag-NPs; (ii) cells with bare HNTs (set A); (iii) cells with added HNTs:Ag-NPs of 5 nm mean size (set C); (iv) cells with added HNTs:Ag-NPs of 10 nm mean size (set E).

Optical extinction spectra and local electric fields in HNTs:Au-NPs were simulated by using Lumerical Finite Difference IDE software (ANSYS, Inc., Canonsburg, PA, USA). The refractive indices of water and HNTs were assumed to be equal to 1.34 and 1.56 in the whole spectral range from 400 to 800 nm. The length, external and internal diameters of HNTs were taken at 1 μm, 80 nm, and 20 nm, respectively. Au- and Ag-NPs were assumed to be randomly distributed on the outer surface of HNTs.

3. Results and Discussion

Figure 1 shows typical TEM images of bare HNTs and those with deposited Au and Ag-NPs of two different mean sizes, i.e., 5 and 10 nm. As seen from Figure 1a, bare HNTs are characterized by an outer diameter of about 50 to 80 nm and a length of about 500 to 1000 nm. Ag- and Au-NPs are randomly distributed on the external surface of HNTs and the size distributions are well-described by the log-normal function (see Figure 1b–e). An individual 10-nm Ag-NP on the HNT's surface is shown in Figure 1f.

The tight binding of plasmonic NPs with HNT' surfaces was confirmed by experiments on prolonged storage of the prepared nanocomposites in water. The size distribution of Ag-NPs was found to be slightly decreased (the mean size changed from 5.4 nm to 4.8 nm) and the LSPR spectrum decreased and spectrally shifted after storage in water for one week [11]. This effect can be explained by the washing out of a part of Ag-NPs due to partial dissolution in water. Additionally, the number of large agglomerates of Ag-NPs became smaller after the storage of the samples in water [11].

Figure 2 shows simulated images of HNTs:Au-NPs and local electric field distribution under illumination with a wavelength close to the LSPR of Au-NPs. The real size distributions of NPs and their concentration are considered during the simulation. It is seen from Figure 2a that the square of the electric field, which is proportional to the local light intensity, increases by an order of magnitude in the vicinity of Au-NPs, especially nearby the NPs' aggregates. Such so-called "hot spots" of the local electric field are responsible for the enhanced plasmonic properties of the prepared nanocomposites.
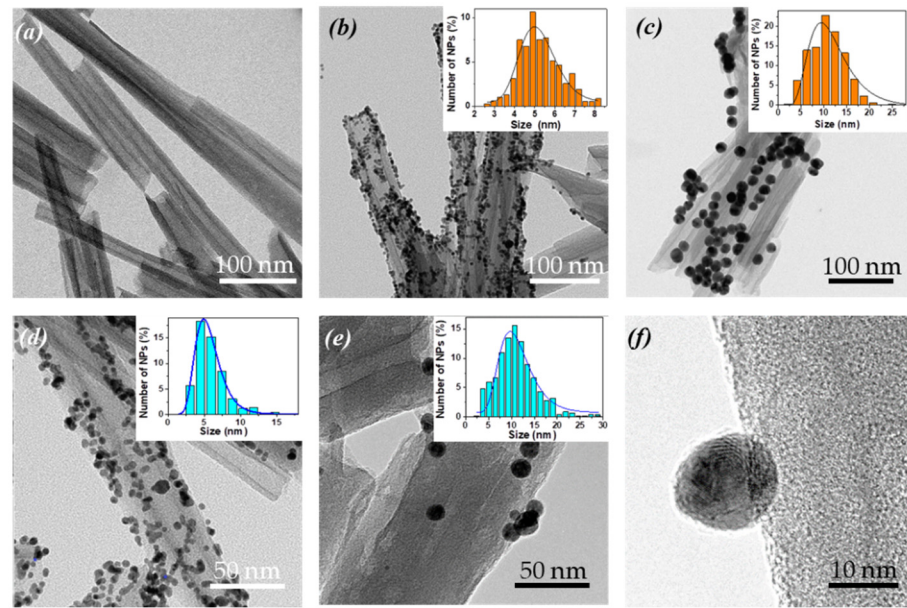
Figure 1. TEM images of (**a**) bare HNTs and (**b**,**c**) HNTs:Au-NPs, (**d**,**e**) HNTs:Ag-NPs, and (**f**) an individual Ag-NP attached on the HNT' surface. The corresponding size distributions for Au (orange bars) and Ag (blue bars) NPs and their fits by log-normal functions (solid lines) are shown in the insets.
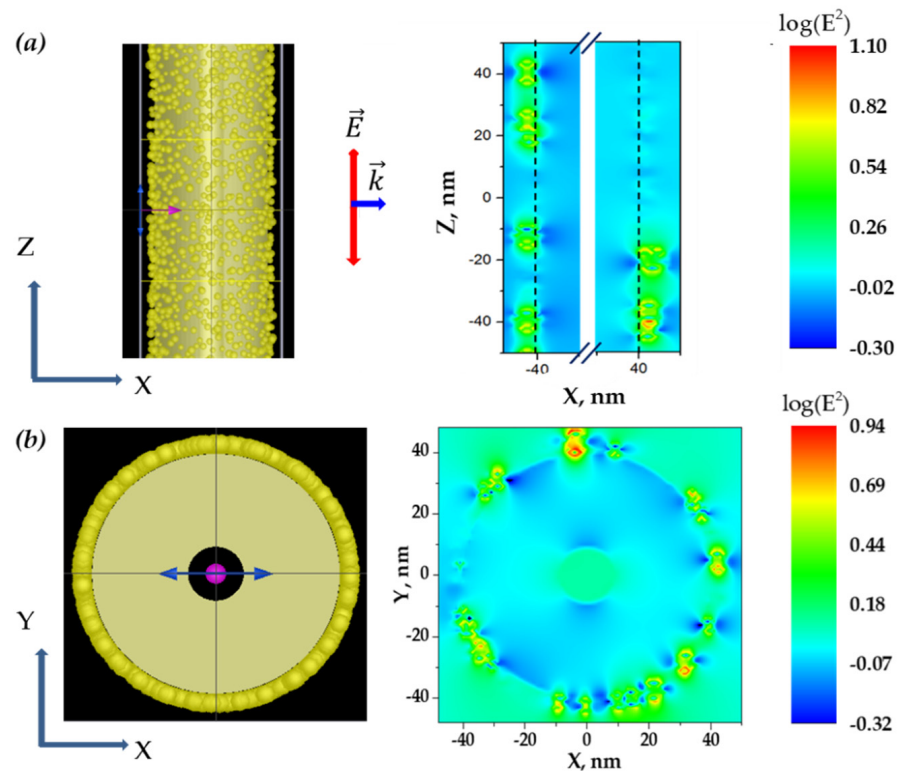
Figure 2. (**a**) Simulation of the HNTs:Au-NPs morphology for randomly distributed Au-NPs (d_0 = 5 nm) and a fragment of the cross-sectional map of the electric field distribution under illumination at 514.5 nm and polarization along the HNT' axis and (**b**) the same simulation for the light polarized in the perpendicular direction. The electric field and wavevector directions are indicated by blue and red arrows in the left-side images. The dashed lines in the right-side images indicate the HNTs' external and internal borders, while the HNTs' center corresponds to X = 0.

The simulated images of HNTs:Ag-NPs and local electric field distributions are shown in Figure 3. The latter reveal numerous "hot spots" of the local electric field nearby NPs. While the strength of the electric field is higher for the field orientation along the HNT axis (Figure 3b), the spatial distribution outside the HNT excited with the perpendicular oriented field is more favorable for the SERS sensing of surrounding biomolecules and cells.
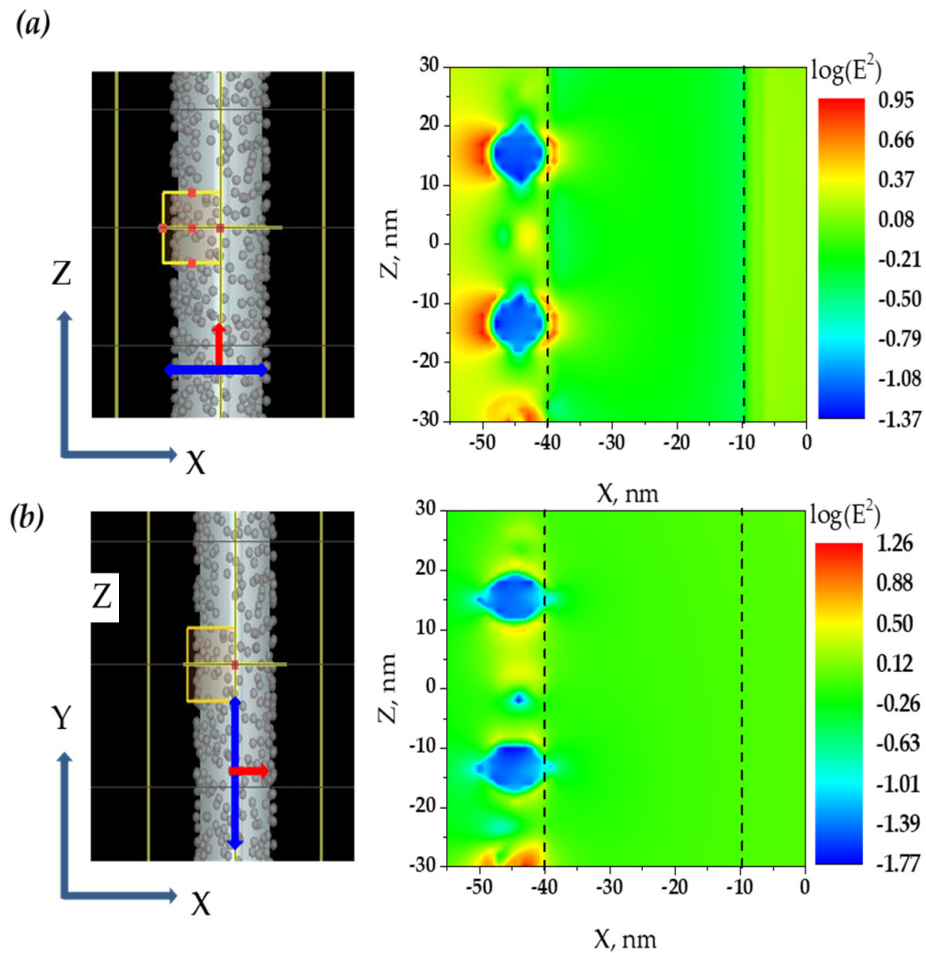
Figure 3. Simulated morphology of HNTs:Ag-NPs for randomly distributed Ag-NPs (d = 10 nm) (left) and fragments of the cross-sectional maps of the electric field distribution (right) under linearly polarized illumination with a wavelength of 632.8 nm; (**a**) the electric field is along the HNT' axis, and (**b**) the electric field is in the perpendicular the HNT' axis. The electric field and wavevector directions are indicated by blue and red arrows in the left-side images. The dashed lines in the right-side images indicate borders of the external and internal surfaces of the nanotube, while its center corresponds to X = 0.

Figure 4 shows simulated extinction spectra of HNTs decorated with Ag- and Au-NPs. HNTs with immobilized monodisperse Au-NPs (d = 10 nm) exhibit a sharp peak of the LSPR with a maximum at 535 nm (see Figure 4a), while the spectrum of the sample with size-distributed NPs is broadened and characterized by a lower extinction value. The larger surface density of metal NPs, the higher the amplitude of LSPR peak. Moreover, the extinction spectra of HNT with attached metal NPs of high surface density exhibit an additional long-wavelength shoulder (see Figure 4b), which can be related to the LSPR of NP's grouping ensembles. The latter is probably also responsible for the formation of "hot spots" shown in Figures 2 and 3. When the size distribution of NPs is considered, the maxima become weaker and broader (compare Figure 4c,d), which is obviously related to the superposition of LSPR from individual NPs and their groping ensembles and agglomerates of various sizes and topology.
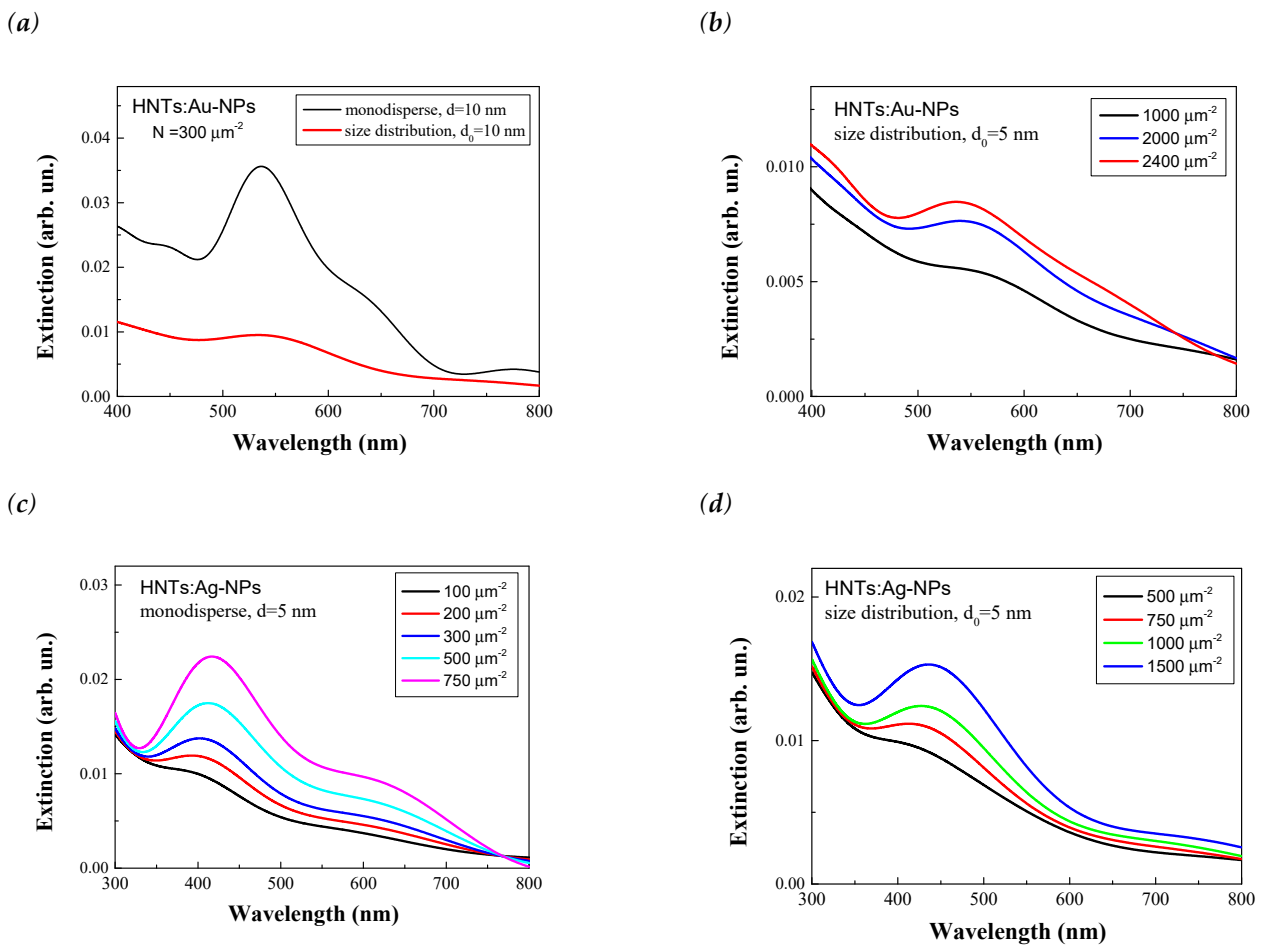
Figure 4. (**a**) Simulated extinction spectra of HNTs with monodisperse (black curve) and size-distributed (red curve) Au-NPs (d = d_0 = 10 nm), which are immobilized on the outer surface of HNTs with surface density of 300 μm^{-1}; (**b**) the same spectra for size-distributed Au-NPs (d_0 = 5 nm) for different surface densities; (**c**) simulated extinction spectra of HNTs:Ag-NPs for randomly distributed monodisperse NPs (d = 5 nm) with different surface density and (**d**) for Ag-NPs with the same mean diameter and size distribution from Figure 1d.

The wide and long-wavelength-shifted extinction spectra of HNTs with densely attached plasmonic NPs are obviously related to the NP grouping ensembles and aggregates, which can create numerous "hot spots" near the HNT's surface where the electric field is enhanced by an order of magnitude at least as shown in Figure 2. The broadening and long-wavelength shift of the extinction spectra of the samples with smaller NPs can be explained by their closer location on the HNT's surface in qualitative agreement with the simulation results (see Figure 2). Indeed, for the same volume concentration, the number of NP groping ensembles increase with decreasing the NP's size, which should lead to a change in the integral shape of LSPR, as shown in Figure 4.

According to the optical transmittance measurements, HNTs with deposited Ag- and Au-NPs exhibit pronounced LSPR in the corresponding spectral regions. Typical extinction spectra of aqueous suspensions of HNT:Ag-NPs and HNT:Au-NPs are shown in Figure 5a,b, respectively. For instance, the LSPR peak in HNTs: Au-NPs is located between 500 and 600 nm and it is more pronounced in the case of bigger Au-NPs (Figure 5b), which is consistent with the results of [29] and our simulations shown in Figure 4. Additionally, when the Au-NPs' diameter decreases from 10 to 5 nm, the LSPR spectrum becomes weaker and broader, which indicates an effect of the interaction between neighboring NPs on the HNT's surface.
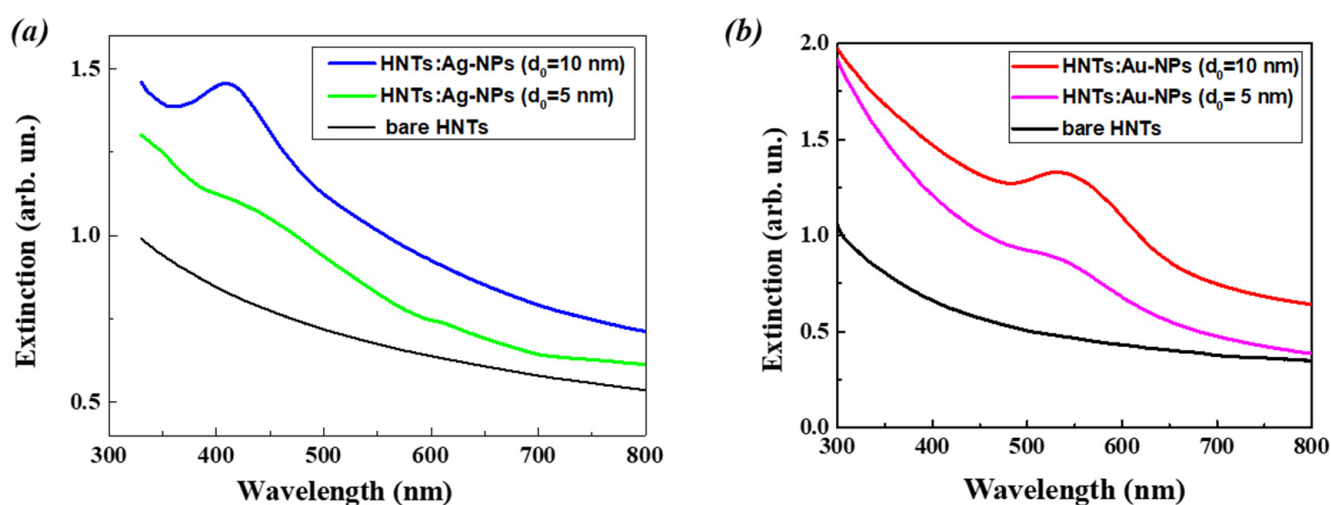
Figure 5. (**a**) Extinction spectra of aqueous suspensions of bare HNTs (black line) and HNTs with deposited Ag-NPs with mean NP's diameters of 5 nm (green line) and 10 nm (blue line); (**b**) extinction spectra of aqueous suspensions of HNTs:Au-NPs with mean diameter of about 5 nm (purple line) and 10 nm (red line) in comparison with bare HNTs (black line). The HNT's concentration was about 1 mg/mL.

Plasmonic fields from NPs deposited on HNTs are well-observed with different biophotonic methods. For example, HNTs:Ag-NPs with added small amounts of probe dye molecules showed a remarkable SERS activity of Ag-NPs even after one week of storage in water, which indicates the improved stability of Ag-NPs on the HNTs' surfaces [11]. The spatial distribution of Ag-NPs on the surface of HNTs forms numerous "hot spots" between NPs that leads to an increase in the SERS efficiency [11–19].

In order to demonstrate the applicability of HNTs:Ag-NPs for biophotonics in vitro, four samples were prepared (see Methods). Figure 6a shows a schematic illustration of the prepared samples and fibroblasts cells cultivated with HNTs:Ag-NPs and Figure 6b,c show optical microscopy images of fibroblast cells and those with added HNTs, respectively. Typical Raman spectra of fibroblasts obtained for the above-mentioned samples of HNTs:Ag-NPs are shown in Figure 6d.

In the case of HNTs:Ag-NPs (set C), the Raman lines, which correspond to the well-known vibrations of proteins in fibroblasts [30,31], are five to six times stronger in comparison to the control sample. This effect was well-reproducible for all obtained spectra. However, even in the presence of bare HNTs (set A), the protein peak intensity was two to three times higher than that in the control sample. This fact can be explained by an increase of elastic light scattering by HNTs that is similar to the well-known Mie scattering. Thus, in addition to the amplification associated with plasmon resonances, there is an additional mechanism associated with light scattering. According to the simulation, a stronger amplification of the Raman signal from cells in the case of HNTs with Ag-NPs of 10 nm (set E) can be expected. However, the intensity for this set is compatible with the intensity observed for set C (d_0 = 5 nm) or even less. The reason for the discrepancy between the expected data and experiment is that the density of the surface coating of HNTs with 10 nm Ag-NPs was rather low since this parameter was not optimized, while the total amount of silver was kept constant for the samples with the mean size of NPs equal to 5 and 10 nm.
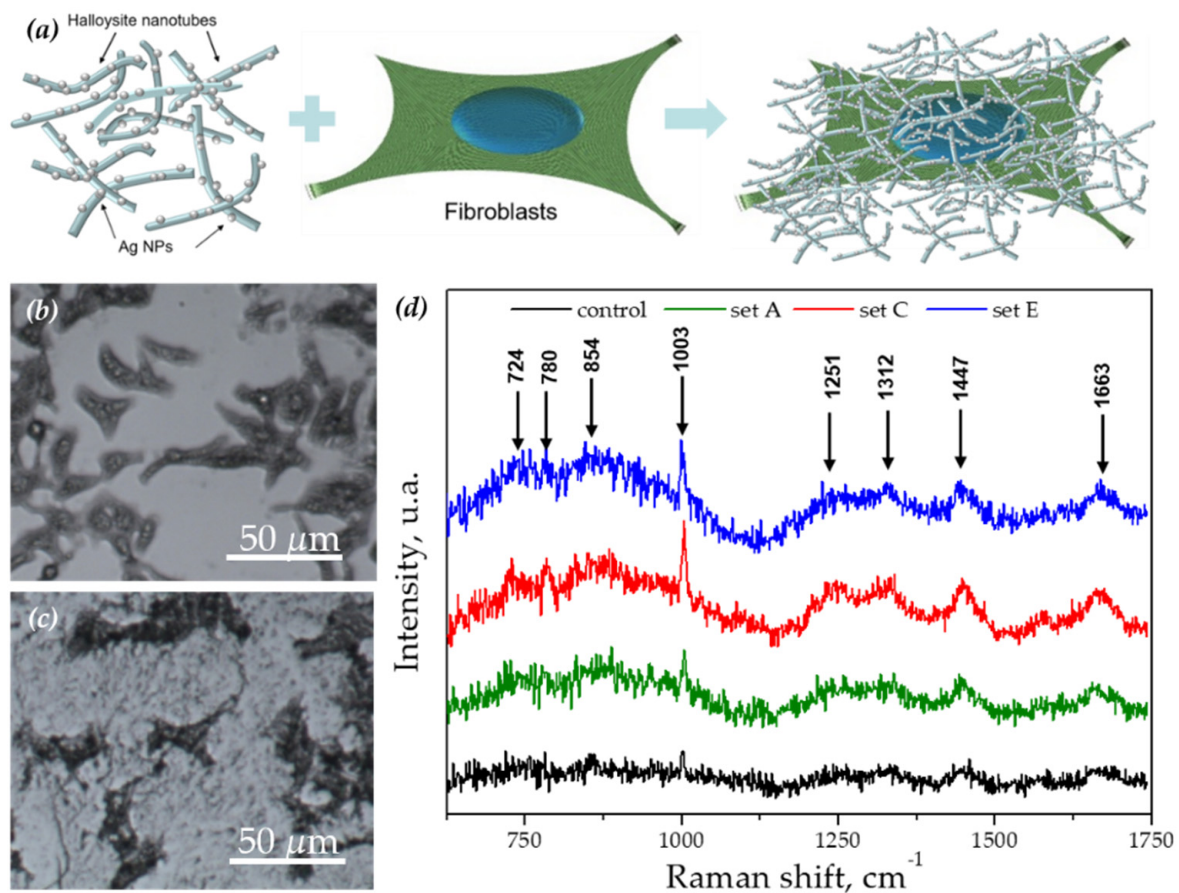
Figure 6. (**a**) Schematic illustration of the sample preparation and fibroblast cells cultivated with HNTs:Ag-NPs; (**b**) optical microscopy images of fibroblasts; (**c**) optical microscopy images of fibroblasts cultivated with HNTs:Ag-NPs; (**c**) Raman spectra of fibroblasts with and without HNTs and HNTs:Ag-NPs. Arrows in panel (**d**) indicate the Raman peaks characteristic of fibroblasts.

4. Conclusions

The obtained results show that gold and silver NPs with sizes from 5 nm to 10 nm randomly distributed on the external surface of HNTs exhibit the localized plasmon resonances in the corresponding spectral regions. The simulated extinction spectra of HNTs with gold and silver NPs are in qualitative agreement with the experimental ones. The simulations reveal an appearance of numerous "hot spots" of the local electric fields nearby NPs. In vitro studies have demonstrated the possibility of enhancing the Raman signal from fibroblast cells by using HNTs:Ag-NPs. Optimization of parameters such as the size of the nanoparticles, their surface density on HNTs, and the concentration of HNTs:Ag-NPs composites added to cells seems to be prospective for an improvement of their properties for the SERS diagnostics of biosystems. Furthermore, the SERS diagnostics can be combined with NP-promoted phototherapy because of the enhanced local electric fields, which stimulate both the direct field-matter interaction in biosystems and the photoinduced heating under irradiation with a wavelength close to the localized surface plasmon resonance.

It seems that the biophotonic modalities of HNTs:(Ag, Au)-NPs should be combined with necessary biofunctionalization of their surfaces to ensure selective binding of those nanocomposites with investigated biosystems. The pronounced plasmonic responses of those nanocomposites allow us to consider them also as potential labels in optical reflection microscopy. Besides their biphotonic applications, HNT-based nanocomposites are of continuing interest in various applications [32–35]. The discussed diagnostics and therapeutic abilities of HNTs with attached plasmonic nanoparticles make them attractive for the development of new biophonic and biomedical methods.

Institutional Review Board Statement: Not applicable.

Informed Consent Statement: Not applicable.

Data Availability Statement: Not applicable.

Conflicts of Interest: The authors declare no conflict of interest.

References

1. Bates, T.F.; Hildebrand, F.A.; Swineford, A. Morphology and structure of endellite and halloysite. *Am. Mineral.* **1950**, *35*, 463–484. Available online: http://www.minsocam.org/ammin/AM35/AM35_463.pdf (accessed on 15 May 2021).
2. Joussein, E.; Petit, S.; Churchman, J.; Theng, B.; Righi, D.; Delvaux, B. Halloysite clay minerals—A review. *Clay Miner.* **2005**, *40*, 383–426. [CrossRef]
3. Gonchar, K.A.; Kondakova, A.V.; Jana, S.; Timoshenko, V.Y.; Vasiliev, A.N. Investigation of halloysite nanotubes with deposited silver nanoparticles by methods of optical spectroscopy. *Phys. Sol. State* **2016**, *58*, 601–605. [CrossRef]
4. Lvov, Y.M.; DeVilliers, M.M.; Fakhrullin, R.F. The application of halloysite tubule nanoclay in drug delivery. *Expert Opin. Drug Deliv.* **2016**, *13*, 977–986. [CrossRef]
5. Lvov, Y.M.; Shchukin, D.G.; Möhwald, H.; Price, R.R. Halloysite Clay Nanotubes for Controlled Release of Protective Agents. *ACS Nano* **2008**, *2*, 814–820. [CrossRef]
6. Vinokurov, V.A.; Stavitskaya, A.V.; Glotov, A.P.; Novikov, A.A.; Zolotukhina, A.V.; Kotelev, M.S.; Gushchin, P.A.; Ivanov, E.V.; Darrat, Y.; Lvov, Y.M. Nanoparticles Formed onto/into Halloysite Clay Tubules: Architectural Synthesis and Applications. *Chem. Rec.* **2018**, *18*, 858–867. [CrossRef] [PubMed]
7. De Jong, W.H.; Borm, P.J. Drug delivery and nanoparticles: Applications and hazards. *Int. J. Nanomed.* **2008**, *3*, 133–149. [CrossRef] [PubMed]
8. Naumenko, E.; Fakhrullin, R. Toxicological evaluation of clay nanomaterials and polymer–clay nanocomposites. *Funct. Polym. Compos. Nanoclays* **2017**, 399–419. [CrossRef]
9. Naumenko, E.; Fakhrullin, R. Halloysite nanoclay/biopolymers composite materials in tissue engineering. *Biotechnol. J.* **2019**, *14*, 1900055. [CrossRef]
10. Guryanov, I.; Naumenko, E.; Akhatova, F.; Lazzara, G.; Cavallaro, G.; Nigamatzyanova, L.; Fakhrullin, R. Selective Cytotoxic Activity of Prodigiosin@halloysite Nanoformulation. *Front. Bioeng. Biotechnol.* **2020**, *8*, 424. [CrossRef] [PubMed]
11. Kornilova, A.V.; Gorbachevskii, M.V.; Kuralbayeva, G.A.; Jana, S.; Novikov, A.A.; Eliseev, A.A.; Vasiliev, A.N.; Timoshenko, V.Y. Plasmonic properties of halloysite nanotubes with immobilized silver nanoparticles for applications in surface-enhanced Raman scattering. *Phys. Status Solidi Appl. Mater. Sci.* **2019**, *216*, 1800886. [CrossRef]
12. Radziuk, D.; Moehwald, H. Highly effective hot spots for SERS signatures of live fibroblasts. *Nanoscale* **2014**, *6*, 6115–6126. [CrossRef]
13. Nika, D.L.; Pokatilov, E.P.; Fomin, V.M.; Devreese, J.T.; Tempere, J. Resonant Terahertz Light Absorption by Virtue of Tunable Hybrid Interface Phonon–Plasmon Modes in Semiconductor Nanoshells. *Appl. Sci.* **2019**, *9*, 1442. [CrossRef]
14. Deshmukh, S.P.; Patil, S.M.; Mullani, S.B.; Delekar, S.D. Silver nanoparticles as an effective disinfectant: A review. *Mater. Sci. Eng. C Mater. Biol. Appl.* **2019**, *97*, 954–965. [CrossRef]
15. Fan, M.; Brolo, A.G. Silver nanoparticles self assembly as SERS substrates with near single molecule detection limit. *Phys. Chem. Chem. Phys.* **2009**, *11*, 7381–7389. [CrossRef] [PubMed]

16. He, R.X.; Liang, R.; Peng, P.; Zhou, Y.N. Effect of the size of silver nanoparticles on SERS signal enhancement. *J. Nanopart. Res.* **2017**, *19*, 267. [CrossRef]

17. Zhan, B.; Liu, C.; Shi, H.; Li, C.; Wang, L.; Huang, W.; Dong, X. A hydrogen peroxide electrochemical sensor based on silver nanoparticles decorated three-dimensional graphene. *Appl. Phys. Lett.* **2014**, *104*, 243704. [CrossRef]

18. Mosier-Boss, P.A. Review of SERS Substrates for Chemical Sensing. *Nanomaterials* **2017**, *7*, 142. [CrossRef]

19. Brazhe, N.A.; Evlyukhin, A.B.; Goodilin, E.A.; Semenova, A.A.; Novikov, S.M.; Bozhevolnyi, S.I.; Chichkov, B.N.; Sarycheva, A.S.; Baizhumanov, A.A.; Nikelshparg, E.I.; et al. Probing cytochrome c in living mitochondria with surface-enhanced Raman spectroscopy. *Sci. Rep.* **2015**, *5*, 13793. [CrossRef]

20. Pan, S.; Gupta, A. Surface-enhanced Solar Energy Conversion Systems Using Gold and Silver Nanoparticles. *Mater. Matters* **2012**, *7*, 64–66. Available online: https://www.sigmaaldrich.com/technical-documents/articles/material-matters/solar-energy-conversion-systems.html (accessed on 15 May 2021).

21. Brazhe, N.A.; Nikelshparg, E.I.; Baizhumanov, A.A.; Grivennikova, V.G.; Semenova, A.A.; Novikov, S.M.; Volkov, V.S.; Arsenin, A.V.; Yakubovsky, D.I.; Evlyukhin, A.B.; et al. SERS uncovers the link between conformation of cytochrome c heme and mitochondrial membrane potential. *bioRxiv* 2021. [CrossRef]

22. Jana, S.; Kondakova, A.V.; Shevchenko, S.N.; Sheval, E.V.; Gonchar, K.A.; Timoshenko, V.Y.; Vasiliev, A.N. Halloysite nanotubes with immobilized silver nanoparticles for anti-bacterial application. *Colloids Surfaces B Biointerfaces* **2017**, *151*, 249–254. [CrossRef] [PubMed]

23. Hong, S.; Li, X. Optimal Size of Gold Nanoparticles for Surface-Enhanced Raman Spectroscopy under Different Conditions. *J. Nanomater.* **2013**, *2013*, 790323. [CrossRef]

24. Langer, J.; Novikov, S.M.; Liz-Marzán, L.M. Sensing using plasmonic nanostructures and nanoparticles. *Nanotechnology* **2015**, *26*, 322001. [CrossRef] [PubMed]

25. Massaro, M.; Colletti, C.G.; Fiore, B.; La Parola, V.; Lazzara, G.; Guernelli, S.; Riela, S. Gold nanoparticles stabilized by modified halloysite nanotubes for catalytic applications. *Appl. Organomet. Chem.* **2018**, *33*, e4665. [CrossRef]

26. Gómez, L.; Hueso, J.L.; Ortega-Liébana, M.C.; Santamaría, J.; Cronin, S.B. Evaluation of gold-decorated halloysite nanotubes as plasmonic photocatalysts. *Catal. Commun.* **2014**, *56*, 115–118. [CrossRef]

27. Zhu, H.; Du, M.L.; Zou, M.L.; Xua, C.S.; Fu, Y.Q. Green synthesis of Au nanoparticles immobilized on halloysite nanotubes for surface-enhanced Raman scattering substrates. *Dalton Trans.* **2012**, *41*, 10465–10471. [CrossRef]

28. Jana, S.; Das, S.; Ghosh, C.; Maity, A.; Pradhan, M. Halloysite nanotubes capturing isotope selective atmospheric CO2. *Sci. Rep.* **2015**, *5*, 8711. [CrossRef]

29. Piella, J.; Puntes, V. Size-Controlled Synthesis of Sub-10-nanometer Citrate-Stabilized Gold Nanoparticles and Related Optical Properties. *Chem. Mater.* **2016**, *28*, 1066–1075. [CrossRef]

30. Surmacki, J.M.; Woodhams, B.J.; Haslehurst, A.; Ponder, B.A.J.; Bohndiek, S.E. Raman micro-spectroscopy for accurate identification of primary human bronchial epithelial cells. *Sci. Rep.* **2018**, *8*, 12604. [CrossRef]

31. Krafft, C.; Dietzek, B.; Popp, J. Raman and CARS microspectroscopy of cells and tissues. *Analyst* **2009**, *134*, 1046–1057. [CrossRef] [PubMed]

32. Luo, Y.; Humayun, A.; Mills, D.K. Surface Modification of 3D Printed PLA/Halloysite Composite Scaffolds with Antibacterial and Osteogenic Capabilities. *Appl. Sci.* **2020**, *10*, 3971. [CrossRef]

33. Lisuzzo, L.; Wicklein, B.; Lo Dico, G.; Lazzara, G.; Del Real, G.; Aranda, P.; Ruiz-Hitzky, E. Functional biohybrid materials based on halloysite, sepiolite and cellulose nanofibers for health applications. *Dalton Trans.* **2020**, *49*, 3830–3840. [CrossRef]

34. Rozhina, E.; Batasheva, S.; Miftakhova, R.; Yan, X.; Vikulina, A.; Volodkin, D.; Fakhrullin, R. Comparative cytotoxicity of kaolinite, halloysite, multiwalled carbon nanotubes and graphene oxide. *Appl. Clay Sci.* **2021**, *204*, 106041. [CrossRef]

35. Lisuzzo, L.; Hueckel, T.; Cavallaro, G.; Sacanna, S.; Lazzara, G. Pickering Emulsions Based on Wax and Halloysite Nanotubes: An Ecofriendly Protocol for the Treatment of Archeological Woods. *ACS Appl. Mater. Interfaces* **2021**, *13*, 1651–1661. [CrossRef] [PubMed]